Design Optimization of a Novel Axial-radial Flux Permanent Magnet Claw Pole Machine with SMC Cores and Ferrite Magnets

Chengcheng Liu, *Member, IEEE*, Fan Yang, Wenfeng Zhang, and Youhua Wang

***Abstract*—Soft magnetic composite (SMC) material is an ideal soft magnetic material employed for developing 3D magnetic flux electromagnetic equipment, due to its advantages of 3D magnetic isotropy characteristic, low eddy current loss, and simple manufacturing process. The permanent magnet claw pole machine (PMCPM) with SMC cores is a good case that the SMC to be adopted for developing 3D flux electrical machines. In this paper, a novel axial-radial flux permanent magnet claw pole machine (ARPMCPM) with SMC cores and ferrite magnets is proposed. Compared with the traditional PMCPM, the proposed ARPMCPM is designed with only one spoke PM rotor and its whole structure is quite compact. For the performance prediction, the 3D finite element method (FEM) is used. Meanwhile, for the performance evaluation, a previously developed axial flux claw pole permanent magnet machine (AFCPM) is employed as the benchmark machine and all these machines are optimized by using the combined multilevel robust Taguchi method. It can be seen that the proposed ARPMCPM is with higher torque/weight density and operation efficiency.**

***Index Terms*—Soft magnetic composite (SMC), Permanent magnetic claw pole machine (PMCPM), Axial-radial flux.**

I. Introduction

SOFT magnetic composite (SMC) material is a relatively new kind of soft magnetic material, which has many advantages over traditional silicon sheets, e.g., the magnetic and thermal isotropic characteristics, low eddy current loss, easy manufacturing process, etc. However it has many disadvantages as well, its permeability is much lower and its hysteresis loss is much higher than that of silicon sheet [1]-[4]. To develop an electrical machine with SMC material, following design guidelines are suggested to be followed, e.g., 3D magnetic flux path, high frequency operation, and permanent magnet excitation [5]-[7].

Manuscript received November 23, 2022; revised January 09, 2023; accepted April 24, 2022. Date of publication December 25, 2023. Date of current version June 30, 2023.

This work was supported by the National Natural Science Foundation of China under project 52007047, and in part by the Outstanding Youth Innovation Project funded by State Key Laboratory of Reliability and Intelligence of Electrical Equipment EERI_OY2021005, and EERI_KF2021014. (*Corresponding author: Chengcheng Liu*)

Chengcheng Liu, Fan Yang, Wenfeng Zhang, and Youhua Wang are with State Key Laboratory of Reliability and Intelligence of Electrical Equipment, School of Electrical Engineering, Hebei University of Technology, Tianjin 300401, China (e-mail: 2016020@hebut.edu.cn, 547905713@qq.com, zhangwf_cas@126.com, wangyi@hebut.edu.cn).

Digital Object Identifier 10.30941/CESTEMS.2023.00041

In the past decades, many electrical machines with SMC cores had been proposed, analyzed, and optimized, mostly for home applications. The SMC has many advantages over traditional silicon sheets, the electrical machines with SMC cores can output better performance than those made by traditional silicon sheets. In which the permanent magnet claw pole machine (PMCPM) has shown its higher torque ability over other electrical machines as it with PM excitation, 3D magnetic flux, and global linear winding configuration [8]-[10]. For most PMCPM, three same single phase PMCPM modules are required with shifting 120 degrees electrically to each other for forming three phase symmetrical operation, and each one phase module has its PM rotor thus the PM utilization is not high [11],[12].

A new axial-radial flux permanent magnet claw pole machine (ARPMCPM) with SMC cores and ferrite magnets is proposed in this paper. Compared with traditional PMCPM, only one PM rotor is required for the proposed machine, therefore the PM utilization is very high. Meanwhile, as two axial flux stator cores are employed, the unbalanced axial force of this machine is reduced, and as both the axial air gap and radial air gap are employed for electromagnetic energy conversion, the torque ability of this machine is high. For the evaluation of the electromagnetic performance, the 3D finite element method (FEM) is employed, and an axial flux claw pole permanent magnet machine (AFCPM) proposed in our previous work is determined as the benchmark machine. For obtaining fair comparison results, all these machines are optimized by using the combined multilevel robust Taguchi method. As seen, the torque/weight density and efficiency of the proposed ARPMCM are higher, therefore it is an ideal machine for low cost home appliance applications.

II. Topology and Operation Principle of ARPMCPM

Fig. 1 shows the main magnetic topology of the proposed ARPMCPM. As shown, the whole machine is composed of two axial flux claw pole stators, one radial flux claw pole stator, one spoke PM rotor in between, and three global windings installed on the axial flux claw pole stator and radial flux claw pole stator respectively. These three claw pole stators are shifted 120 electric degrees with each other. For obtaining good operation performance, the sectional area of the winding needs to be designed appropriately for achieving three phase symmetrical operation. Both the claw pole stators and rotor cores are made

by using the SMC material. For the PMs, the ferrite magnet material is selected, and they are all magnetized along the circumference direction, in addition, the magnetization direction of adjacent PMs is opposite.

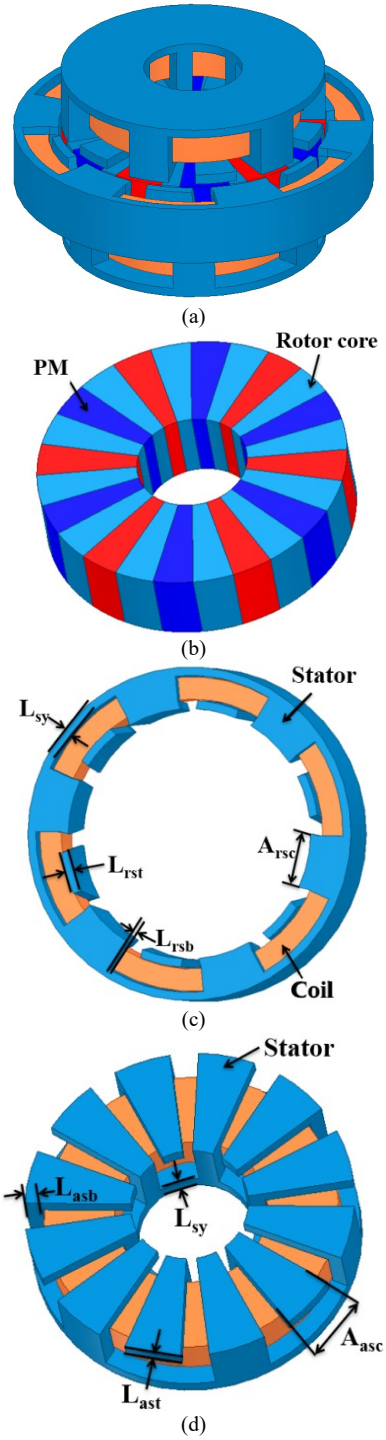

Fig. 1. (a) Topology of ARPMCPM. (b) Rotor cores and PM. (c) Radial flux claw pole stator. (d) Axial flux claw pole stator.

The main operation principle of ARPMCPM is quite similar to that of PMCPM, the main difference is that the proposed ARPMCPM can employ both the axial air gap flux and radial air gap flux, the main magnetic flux path is shown in Fig. 2. With employing this kind of topology the different phases are not independent on each other and they are a coupled structure.

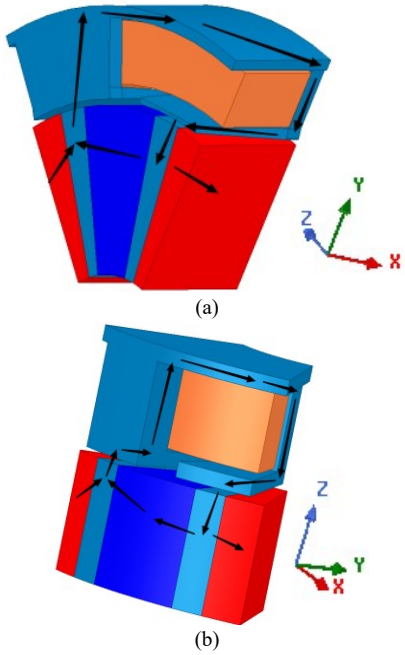

Fig. 2. (a) Radial flux path of ARPMCPM. (b) Axial flux path of the ARPMCPM.

III. Robust Design Based on Taguchi Method

As the sectional area of the winding determines the electric loading and the main structure of the proposed ARPMCPM is non-symmetry, for achieving relatively better machine performance their main dimensions and parameters are optimized. The corresponding parameters for design optimization are shown in Fig. 1, which includes the teeth thickness of the radial claw pole stator (L_{rst}), the side wall thickness of the radial claw pole stator (L_{rsb}), the teeth thickness of axial claw pole stator (L_{ast}), the side wall thickness of axial claw pole stator (L_{asb}), the inner radius of radial claw pole stator (R_{rsi}), rotor inner radius (R_{ri}), teeth width angle of radial claw pole stator (A_{rsc}), teeth width angle of axial claw pole stator (A_{asc}) and angle of PM (A_{pm}) are determined as the main parameters for optimization.

Regarding the design optimization of ARPMCPM is a high-dimensional design optimization problem, the multilevel optimization method, and robust Taguchi method are combined for the design optimization for reducing the computation cost [13]-[15]. Fig. 3 shows the flowchart of the combined multilevel robust Taguchi method.

First: Based on the obtained sensitivity analysis results, 9 design parameters of one high dimensional problem are divided into 4 design parameters and 5 design parameters of two relatively low dimensional problems.

Second: Use the robust Taguchi method to find an optimal design for each low dimensional design optimization problem in each level. Specifically, the orthogonal arrays (with 4 levels for all parameters) are created and employed to find the best level for all parameters.

Third: Optimize the divided two low-dimensional problems in a sequential way, specifically repeating the optimization process unless the relative error of the objective calculated from two optimization loops is lower than 0.5%.

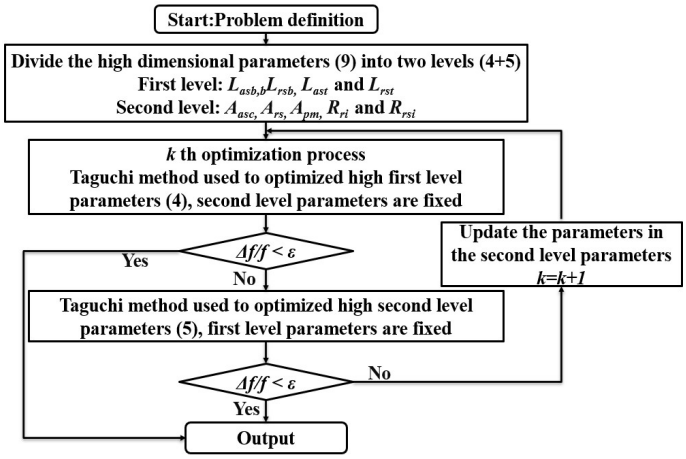

Fig. 3. Flowchart of the combined multilevel robust Taguchi method.

TABLE I
SAMPLES FOR LSA AND AVERAGE SENSITIVITIES FOR ALL PARAMETERS

Parameter	Amplitude variation of parameter					Average sensitivity
	-20%	-10%	0	10%	20%	
A_{asc}/deg	19.2	21.6	24	26.4	28.8	0.03
A_{rsc}/deg	19.2	21.6	24	26.4	28.8	0.03
A_{pm}/deg	8	9	10	11	12	0.06
L_{asb}/mm	3.2	3.6	4	4.4	4.8	0.15
L_{rsb}/mm	3.2	3.6	4	4.4	4.8	0.24
L_{ast}/mm	3.2	3.6	4	4.4	4.8	0.19
L_{rst}/mm	3.2	3.6	4	4.4	4.8	0.42
R_{ri}/mm	12	13.5	15	16.5	18	0.02
R_{rsi}/mm	32	36	40	44	48	0.04

Table I tabulates the 37 samples and the average local sensitivity analysis (LSA) results for 9 design parameters of ARPMCPM. Meanwhile, the normalized average sensitivity value is employed for making the obtained sensitivity values comparable. Through ranking these calculated sensitivity values, L_{rst}, L_{rsb}, $L_{ast,}$ and L_{asb} are assigned to the first level, while the other design parameters are to the second level.

The robust Taguchi method is used to optimize these parameters in the first level and then sequentially the parameters in the second level are optimized. The initial values and range for the design parameters are tabulated in Table II. The control parameters, the noise factors, and the corresponding design values are tabulated in Table III. Each control component has 4 levels, and each noise factor has two levels, as illustrated.

TABLE II
DESIGN PARAMETERS AND RANGES

Parameter	Unit	Initial	Min	Max
L_{rst}	mm	5	3	8
L_{asb}	mm	4	3	8
L_{ast}	mm	3.5	3	8
L_{rsb}	mm	6	3	8

TABLE III
DESIGN PARAMETERS AND RANGES

Control factor	Unit	Levels				Noise factor	Levels	
		1	2	3	4		1	2
L_{rst}	mm	3	3.5	4	4.5	ΔL_{rst}	+0.10	-0.10
L_{asb}	mm	3.5	4	4.5	5	ΔL_{asb}	+0.10	-0.10
L_{ast}	mm	3.5	4	4.5	5	ΔL_{ast}	+0.10	-0.10
L_{rsb}	mm	3.5	4	4.5	5	ΔL_{rsb}	+0.10	-0.10

Based on these developed control and noise factors, an orthogonal array is built as shown in Table IV. 16 rows are formed to establish the internal array, and 8 columns are formed to establish the external array, where the internal array represents the control factors, while the external array represents the noise factors. Therefore, for the performance calculation, 128 combinations will be required.

TABLE IV
THE ORTHOGONAL ARRAY AND OBJECTIVE VALUES FOR ARPMCPM

	Control factors				Noise factors							
	1	**2**	**3**	**4**	**1111**	**1112**	**1221**	**1222**	**2121**	**2122**	**2211**	**2222**
1	1	1	1	1	1.882	1.923	1.827	1.890	1.861	2.011	1.887	1.826
2	1	2	2	2	1.939	1.890	1.924	1.906	1.835	2.011	1.801	1.891
3	1	3	3	3	2.137	1.968	1.993	1.929	2.144	2.142	2.077	1.961
4	1	4	4	4	2.315	2.096	2.146	2.379	2.225	2.217	2.359	2.138
5	2	1	2	3	2.219	2.049	1.930	2.204	2.279	2.272	2.135	2.071
6	2	2	1	4	1.790	1.881	1.743	1.885	1.949	1.840	2.023	1.926
7	2	3	4	1	1.821	1.890	1.851	2.092	1.881	1.910	1.981	1.914
8	2	4	3	2	1.840	1.739	1.755	1.573	1.751	1.737	1.692	1.612
9	3	1	3	4	2.244	2.239	2.332	2.199	2.454	2.383	2.636	2.294
10	3	2	4	3	2.458	2.194	2.236	2.118	2.473	2.412	2.386	2.328
11	3	3	1	2	2.116	1.911	2.076	2.038	2.120	2.046	2.206	1.986
12	3	4	2	1	1.994	1.938	1.907	1.899	1.990	1.849	2.028	1.908
13	4	1	4	2	2.747	2.756	2.550	2.664	2.874	3.070	3.092	2.919
14	4	2	3	1	2.893	2.498	2.488	2.676	2.413	2.815	2.615	2.635
15	4	3	2	4	2.215	2.268	2.281	2.177	2.391	2.357	2.204	2.341
16	4	4	1	3	2.208	2.127	2.175	1.968	2.204	2.027	2.173	1.996

By using the FEM package ANSYS MAXWELL 3D, both the average torque and the torque ripple can be calculated. To

find the best design sample, the following objective function is defined

$$y(i,j)=1.5\frac{T_{\text{ave}_{\text{initial}}}}{T_{\text{ave}(i,j)}}+0.5\frac{T_{\text{rip}(i,j)}}{T_{\text{rip}_{\text{initial}}}} \quad (1)$$

where T_{ave} is the average torque, T_{rip} is torque ripple, the subscript of initial represents the corresponding performance obtained from the initial design, and the i (1, 2, 3. . , 16) and j (1, 2, 3. . . , 8) are the design samples with the corresponding control and noise factors respectively. Table IV lists the calculated objective values for these 128 simulations.

For obtaining the S/N ratio, two main steps need to be done. Firstly, the S/N ratio for each row of the internal array needs to be calculated. In this paper, as the objective function is the smaller the better, the following calculation equation is used

$$SN(i)=-10\times\lg\left[\frac{1}{8}\times\sum_{j=1}^{8}y^2(i,j)\right] \quad (2)$$

Secondly, based on the calculated S/N ratio as shown in Table V, the average value in each parameter level is determined, as tabulated in Table VI.

TABLE V
S/N RATIOS FOR INTERNAL ARRAYS

	S/N ratios		S/N ratios
1	-5.53	9	-7.43
2	-5.58	10	-7.34
3	-6.22	11	-6.29
4	-6.99	12	-5.76
5	-6.64	13	-9.07
6	-5.49	14	-8.41
7	-5.66	15	-7.16
8	-4.68	16	-6.49

TABLE VI
AVERAGE S/N RATIO IN EACH LEVEL FOR CONTROL FACTORS

Factor	Level	S/N ratio	Factor	Level	S/N ratio
L_{rst}	1	-6.08	L_{ast}	1	-5.95
	2	-5.62		2	-6.28
	3	-6.70		3	-6.68
	4	-7.78		4	-7.27
L_{asb}	1	-7.16	L_{rsb}	1	-6.34
	2	-6.71		2	-6.40
	3	-6.33		3	-6.67
	4	-5.98		4	-6.77

The obtained average S/N ratios for all levels of each control factor are illustrated in Fig. 4. As mentioned before, the design target in this paper is the smaller the better, therefore the best level of each factor is the one that has the highest S/N ratio. Thus, levels 2, 4, 1, and 1 are the best ones for these four control factors, respectively. Specifically, the average torque is 1.73 Nm and the torque ripple is 89.7% when the ARPMCPM with this optimal design, is much better than those of the ARPMCPM with the initial design (1.31Nm and 172%).

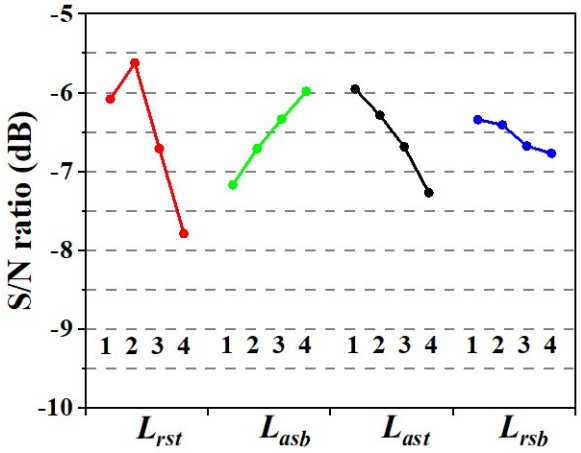

Fig. 4. S/N ratio in each factor.

By using the Taguchi method, the optimal design can be found, and the optimized objectives can be obtained for this round. For obtaining the best design, the sequential optimization design is employed, then the levels for each control factor will be updated with new levels, and the new optimal design can be obtained. Comparing two optimal objectives when their difference is lower than 0.5%, the optimization process will end and determine the value of the first level parameter. Otherwise, the levels will be updated furthermore, and the Taguchi method will be adopted again. By using the same optimization method, the second level has been optimized. The optimization processes of ARPMCPM are illustrated in Fig. 5.

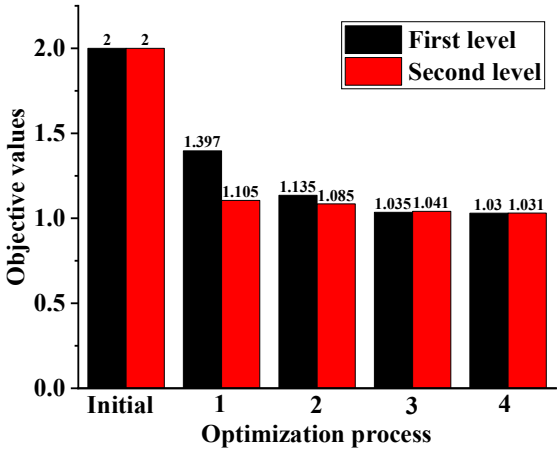

Fig. 5. Optimization processes of ARPMCPM.

By using the above method, the final dimensions of ARPMCPM are determined as shown in Table VII. By adopting the combined multilevel robust Taguchi method, the average torque and the torque ripple of the optimized ARPMCPM are 2.24 Nm and 52.7% respectively, which are much better than the ARPMCPM with the initial design (1.31 Nm and 172%). Through the comparison, it can be seen that the average torque has increased by about 71.0%, while the torque ripple and the objective value have decreased by about 69.0% and 48.5% respectively.

TABLE VII
MAIN PARAMETERS OF ARPMCPM

Parameter	Symbol /Unit	Initial design	Optimal design
Radial stator outer radius	R_{rso}/mm	60.0	60.0
Radial stator inner radius	R_{rsi}/mm	40.0	45.0
Rotor inner radius	R_{ri}/mm	15.0	16.5
Angle of radial stator claw pole	A_{rsc}/deg	22.0	23.6
Angle of axial stator claw pole	A_{asc}/deg	22.0	18.1
Angle of PM	A_{pm}/deg	20.00	22.0
Thickness of radial stator claw pole	L_{rst}/mm	5.00	3.00
Thickness of radial stator side wall	L_{rsb}/mm	6.00	3.01
Thickness of axial stator claw pole	L_{ast}/mm	3.50	3.47
Thickness of axial stator side wall	L_{asb}/mm	4.00	7.28
Thickness of stator yoke	L_{sy}/mm	3.00	3.00
Air gap length	L_{gap}/mm	1.00	1.00
Axial length	L_{axial}/mm	64.6	64.6
Number of coil turns	N_c	100	100
Number of pole pairs	N_p	6	6
Slot fill factor	/	0.6	0.6
Torque	T/Nm	1.31	2.24
Torque ripple	/	172%	52.7%
Objective value	/	2.00	1.03

IV. ELECTROMAGNETIC PARAMETERS ANALYSIS AND OVERALL PERFORMANCE

Based on the 3D FEM, the no load magnetic field distribution and the main electromagnetic parameters of ARPMCPM can be calculated. In this paper, the 3D Maxwell is adopted for the FEM calculation, the calculation time is about 75 minutes for a static analysis and 18 minutes for a transient analysis based on a workstation with the CPU of E5, for each sample.

Fig. 6 shows the no load magnetic flux density distributed on the ARPMCPM. As shown, the maximum flux density occurs on the wall and teeth of the claw pole stator. The maximum magnetic flux density on the stator teeth is about 1.5 T, though the low co-energy ferrite magnet is employed. Compared with the axial flux claw pole stator, the radial flux claw pole stator has higher magnetic flux density distribution.

Fig. 7 shows flux density distribution in the axial air gap and radial air gap. As shown, the maximum value of air gap flux density is about 0.64 T, and the radial air gap flux density distribution is similar to the axial air gap flux density distribution.

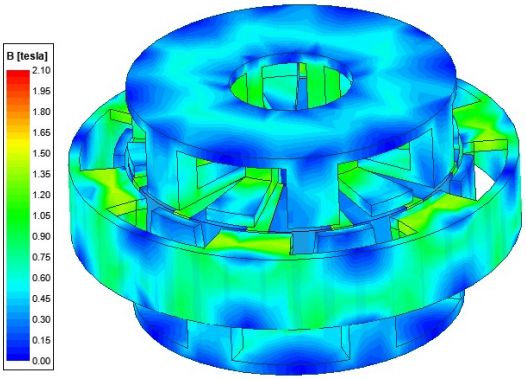

Fig. 6. No load flux density distribution of ARPMCPM.

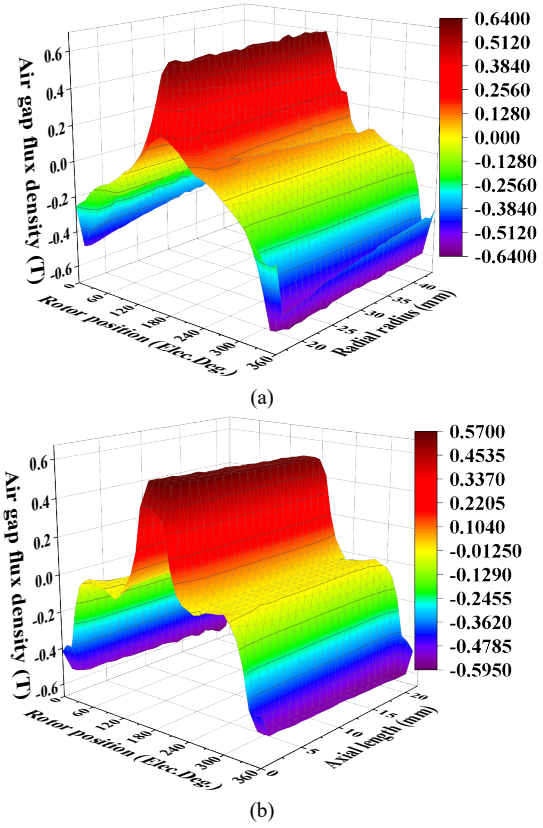

Fig. 7. (a) Axial air gap flux density distribution. (b) Radial air gap flux density distribution.

For determination of the performance of the PM machine, the electromagnetic parameters, e.g., the PM flux linkage, inductance, and cogging torque are very important. Fig. 8(a) shows the no load three phase PM flux linkage waveform. It can be seen that the magnitude of the A phase PM flux linkage is slightly higher than the other PM flux linkages. The main reason is that the main structure of the proposed machine is non-symmetry, and A phase winding is located on the radial flux claw pole stator. Fig. 8(b) shows the self-inductance waveform comparison. The B phase and C phase self-inductance are equal, while the A phase self-inductance is higher than the others. The main reason is that the B phase and C phase have the same stator structure.

The cogging torque is generally produced by the interaction between the magnetic field and the slots, which is an inherent disadvantage of the PM machine that affects the machine's performance. Though the average of the cogging torque is zero in a complete period, it produces the torque ripple. Fig. 8(c) shows the calculated cogging torque versus the rotor position. As shown, its peak value is about 0.45 Nm, which can bring the ARPMCPM with very high vibration and noise, its reduction will be presented in future work. Fig. 8(d) shows the average torque versus the applied current density. As shown the torque increases with the current density linearly when the current density is below 4 A/mm^2. However, when the applied current density is high, the ratio of torque to current will decrease as the wall and teeth of the claw pole stator will be saturated. Fig. 8(e) shows the electromagnetic torque waveform. As shown, the average torque is about 2.24 Nm with the applied current density of 6 A/mm^2. It can be seen that the torque ripple is about

52.7%, which is higher than the cogging torque.

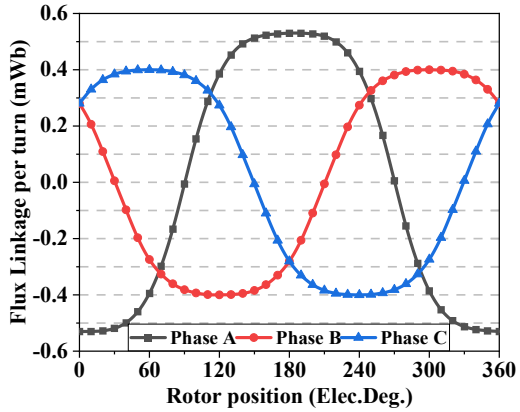

(a)

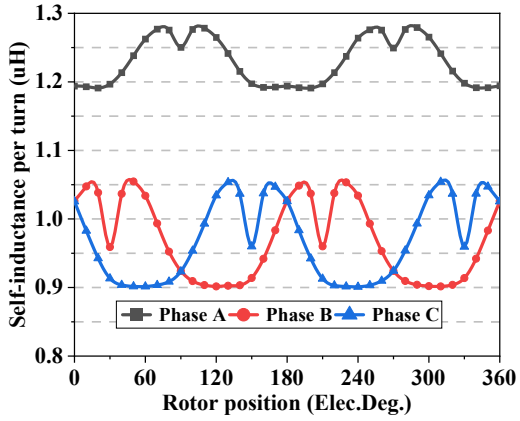

(b)

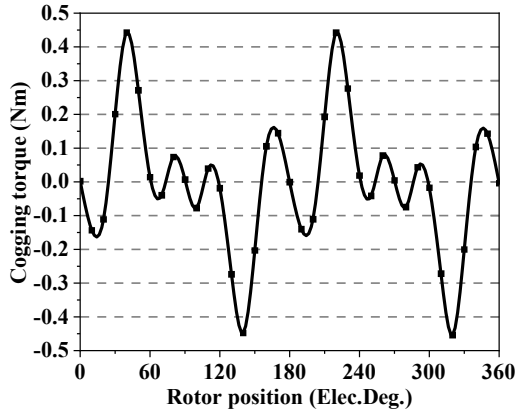

(c)

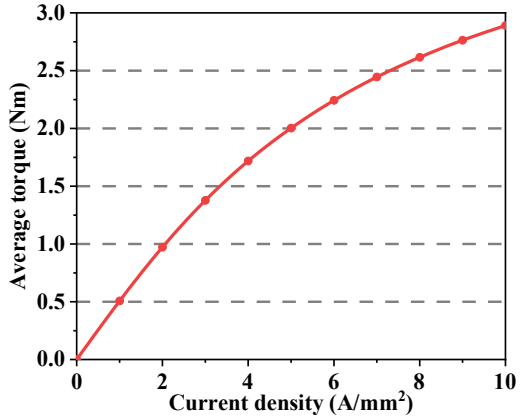

(d)

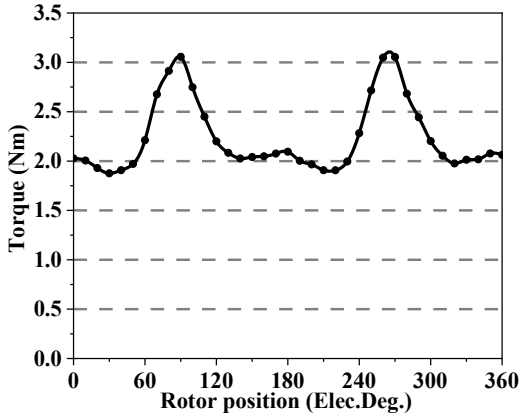

(e)

Fig. 8. Main magnetic parameters of ARPMCPM. (a) PM flux linkage per turn. (b) Self-inductance. (c) Cogging torque. (d) Average torque versus applied current. (e) Torque waveform.

Efficiency map is very important for evaluating the main performance of an electrical machine, as it can show machine performance under different working conditions. The efficiency can be calculated by

$$\eta = \frac{P_{\text{out}}}{P_{in}} = \frac{P_{\text{em}} - P_{\text{core}} - P_{\text{mech}}}{P_{\text{em}} + P_{\text{copper}}} \tag{3}$$

where P_{out}, P_{in}, P_{em}, P_{core}, P_{mech} and P_{copper} are output power, input power, electromagnetic power, core loss, mechanical loss, and copper loss respectively. The mechanical loss is estimated to equal about 1.5% of the output power.

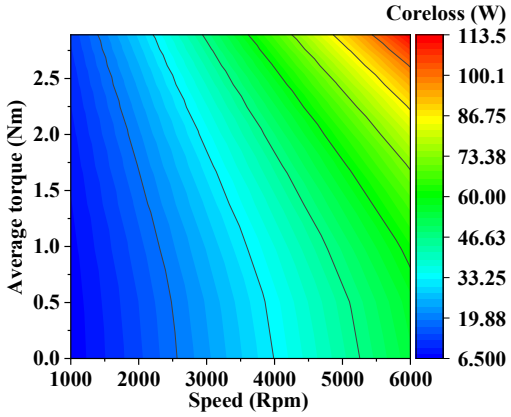

(a)

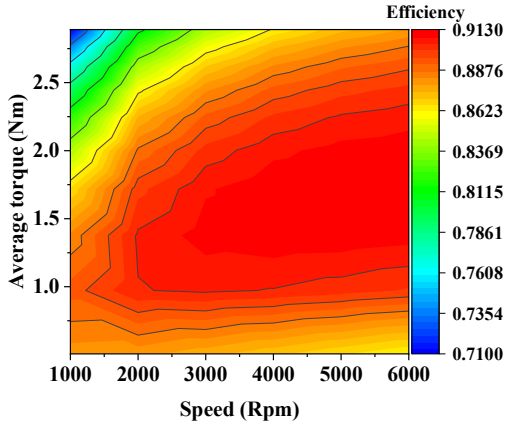

(b)

Fig. 9. (a) Core loss map. (b) efficiency map.

Fig. 9(a) shows the calculated core loss of ARPMCPM varied with the rotor speed and torque. As no reluctance torque can be adopted for this machine, for the machine control the d-axis current is set to zero. It can be seen that the calculated core loss increases quickly with the operating frequency increases. Fig. 9(b) shows the calculated efficiency map of ARPMCPM. As shown, the maximum efficiency equals about 0.913, and the high efficiency operation region is wide.

For evaluating the main performance of the proposed ARPMCM fairly, an axial flux claw pole permanent magnet machine (AFCPM) is determined as the benchmark machine [16]. Fig. 10 shows the main topology of AFCPM. For achieving fair comparison results, the main parameters of these two machines are optimized with the same outer volume based on the combined multilevel robust Taguchi method.

Table VIII tabulates the main performance comparison of these two electrical machines under the rated working conditions, specifically the current density of 6 A/mm^2 and the rotor speed of 1000 rpm, based on the 3D-FEM. The mass of ARPMCPM is much lower than that of AFCPM, as its outer radius of the axial flux claw pole stator is much lower than its overall outer radius. As shown, though the torque ripple of the proposed ARPMCPM is higher than that of AFCPM, its torque density, and efficiency are higher as well. And the cogging torque of ARPMCPM is less than that of AFCPM. As shown, the overall performance of the ARPMCPM is better than that of AFCPM, except for the torque ripple. Therefore the proposed ARPMCPM can be developed for low cost applications with relatively good performance.

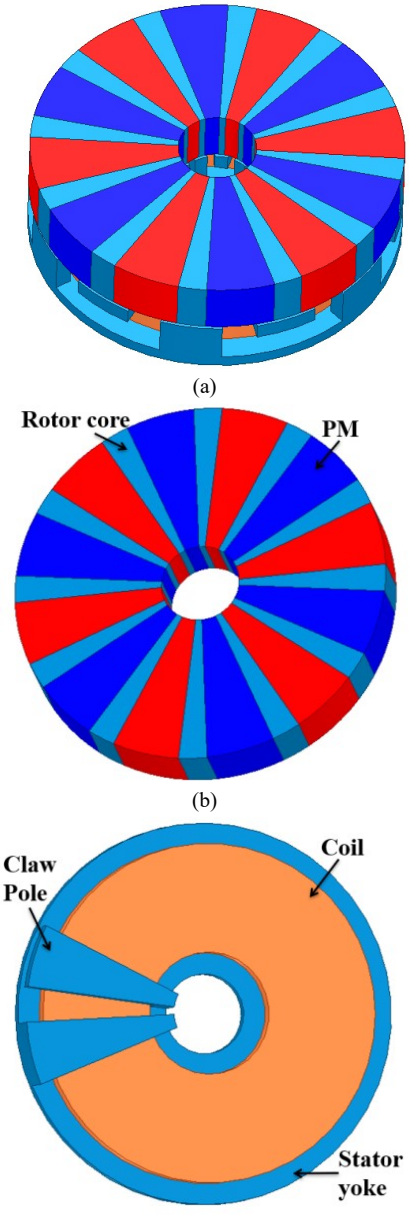

(a) (b) (c)

(d)

Fig. 10. (a) Topology of AFCPM. (b) rotor core and PM. (c) claw poles, coil, and stator yoke. (d) complete stator.

TABLE VIII
PERFORMANCE COMPARISON

Item	AFCPM	ARPMCPM
Power (W)	225	259
Torque (Nm)	1.81	2.24
Torque ripple (%)	27.3	52.7
Cogging torque (Nm)	1.10	0.90
Torque per unit weight (Nm/kg)	0.48	0.94
Torque per unit PM weight (Nm/kg)	1.55	5.60
Efficiency	0.81	0.82
PM Mass (kg)	1.17	0.40
Mass (kg)	3.79	2.37

V. CONCLUSION

A novel ARPMCPM is proposed and analyzed in this paper. As both the axial air gap and radial air gap are employed for the electromagnetic energy transformation, the PM utilization of this machine is very high. The combined multilevel robust Taguchi method is employed for determining the main design parameters. Compared with the benchmark AFCPM, the torque/weight density, and efficiency of the proposed ARPMCPM are higher. Therefore, the proposed machine is an ideal machine for low cost home appliance applications.

REFERENCES

[1] D. Gumbleton-Wood, G. J. Atkinson, and L. Sjöberg, "Electromagnetic Properties of Soft Magnetic Composites and Electrical Steels at High Frequencies Considering Material Manufacturing Techniques," in *Proc. of 2019 IEEE International Electric Machines & Drives Conference (IEMDC)*, San Diego, CA, USA, 2019, pp. 2027-2034.

[2] A. Krings, A. Boglietti, and A. Cavagnino *et al*, "Soft Magnetic Material Status and Trends in Electric Machines," *IEEE Transactions on*

Industrial Electronics, vol. 64, no. 3, pp. 2405-2414, March 2017.

[3] E. Pošković, L. Ferraris, and F. Franchini *et al*, "SMC Materials in Electrical Machine Prototypes," in *Proc. of 2019 IEEE International Electric Machines & Drives Conference (IEMDC)*, San Diego, CA, USA, 2019, pp. 2042-2047.

[4] Y. J. Li, Q. X. Yang, and Y. H. Wang *et al*, "Rotational core loss features of soft magnetic composite materials under excitation frequencies from 5 Hz to 1000 Hz," in *Proc. of 2013 IEEE International Conference on Applied Superconductivity and Electromagnetic Devices*, Beijing, China, 2013, pp. 450-453.

[5] Y. Guo, J. Zhu, and H. Lu *et al*, "Design considerations of electric motors with soft magnetic composite cores," in *Proc. of 2016 IEEE 8th International Power Electronics and Motion Control Conference (IPEMC-ECCE Asia)*, Hefei, China, 2016, pp. 3007-3011.

[6] M. Ozeki, and S. Shimomura, "Comparative study of integrated radial-axial flux rotor motor using ferrite magnet," in *Proc. of 2017 20th International Conference on Electrical Machines and Systems (ICEMS)*, Sydney, NSW, Australia, 2017, pp. 1-6.

[7] M. A. Noroozi Dehdez, and J. Milimonfared, "A Novel Radial–Axial Flux Switching Permanent Magnet Generator," *IEEE Transactions on Industrial Electronics*, vol. 69, no. 12, pp. 12096-12106, Dec. 2022.

[8] J. G. Zhu, Y. G. Guo, and Z. W. Lin *et al*, "Development of PM Transverse Flux Motors With Soft Magnetic Composite Cores," *IEEE Transactions on Magnetics*, vol. 47, no. 10, pp. 4376-4383, Oct. 2011.

[9] Y. Guo, J. Zhu, and P. A. Watterson *et al*, "Development of a PM transverse flux motor with soft magnetic composite core," *IEEE Transactions on Energy Conversion*, vol. 21, no. 2, pp. 426-434, June 2006.

[10] B. Ma, G. Lei, and J. Zhu *et al*, "Design Optimization of a Permanent Magnet Claw Pole Motor With Soft Magnetic Composite Cores," *IEEE Transactions on Magnetics*, vol. 54, no. 3, pp. 1-4, Mar. 2018.

[11] Chengcheng Liu, Dongyang Wang, and Shaopeng Wang *et al*, "Design and Analysis of a New Permanent Magnet Claw Pole Machine with S-shape Winding," *IEEE Transactions on Magnetics*, vol. 57, no. 2, pp. 1-5, Feb. 2021.

[12] W. Zhang, Y. Xu, and M. Sun, "Design of a Novel Claw Pole Transverse Flux Permanent Magnet Motor Based on Hybrid Stator Core," *IEEE Transactions on Magnetics*, vol. 57, no. 6, pp. 1-5, June 2021.

[13] G. Lei, G. Bramerdorfer, and C. Liu *et al*, "Robust Design Optimization of Electrical Machines: A Comparative Study and Space Reduction Strategy," *IEEE Transactions on Energy Conversion*, vol. 36, no. 1, pp. 300-313, Mar. 2021.

[14] G. Lei, W. Xu, and J. Hu *et al*, "Multilevel Design Optimization of a FSPMM Drive System by Using Sequential Subspace Optimization Method," *IEEE Transactions on Magnetics*, vol. 50, no. 2, pp. 685-688, Feb. 2014.

[15] X. Sun, Z. Shi, and G. Lei *et al*, "Multi-Objective Design Optimization of an IPMSM Based on Multilevel Strategy," *IEEE Transactions on Industrial Electronics*, vol. 68, no. 1, pp. 139-148, Jan. 2021.

[16] Chengcheng Liu, Xue Li, and Gang Lei *et al*., "Performance Evaluation of an Axial Flux Claw Pole Machine With Soft Magnetic Composite Cores," *IEEE Transactions on Applied Superconductivity*, vol. 28, no. 3, pp. 1-5, April 2018.

Chengcheng Liu (S'14 – M'16) was born in Jiangsu, China in 1988. He received the B.E. degree in automation engineering from Yangzhou University, Yangzhou, China, in 2010 and the Ph.D. degree in electrical engineering from Hebei University of Technology, Tianjin, China, in 2016. He was a joint Ph.D. student supported by the Chinese scholarship council in the University of Technology, Sydney, Australia.

He is currently an associate professor at Hebei University of Technology, Tianjin, China. His research interests include the design, analysis, control and optimization of electromagnetic devices.

Fan Yang was born in China on November 1998. He received the B.E. degree in Electrical Engineering from Hebei University of Science and Technology, Hebei, China, in 2020. He is currently pursuing the M.E. degree in electrical engineering at Hebei University of Technology, Tianjin, China.

His current research interests include design and optimization of electromagnetic devices.

Wenfeng Zhang was born in Handan, Hebei province, China, in 1985. He received his Bachelor's degree degree in electric engineering from Hebei Normal University of Science and Technology, China, in 2008, Master's Degree in electrical engineering from Hebei University of Technology, China, in 2011, and Doctor's degree in electrical engineering from University of Chinese Academy of Sciences. His research interests include designing of electric machines and applied superconductivity, e.g., HTS generator and induction heater.

Youhua Wang received the B.E. degree from Xian Jiaotong University, Xian, China, in 1987; the M.E. degree from the Hebei University of Technology, Tianjin, China, in 1990; and the Ph.D. from Fuzhou University, Fuzhou, China, in 1994, all in electrical apparatus.

He is currently a Professor at the College of Electrical Engineering. His current research interests include measurement and modeling of properties of magnetic materials, numerical analysis of the electromagnetic field, and electromagnetic device design, analysis and optimization.